J Appl Physiol 124: 564–572, 2018.
First published July 13, 2017; doi:10.1152/japplphysiol.00297.2017.

REVIEW | *Emerging Wearable Physiological Monitoring Technologies & Decision Aids for Health & Performance*

Wearable brain imaging with multimodal physiological monitoring

Gary E. Strangman,[1,2,3] Vladimir Ivkovic,[1] and Quan Zhang[1,2]

[1]*Neural Systems Group, Massachusetts General Hospital, Harvard Medical School, Charlestown, Massachusetts;* [2]*Center for Space Medicine, Baylor College of Medicine, Houston, Texas; and* [3]*Translational Research Institute, Houston, Texas*

Submitted 3 April 2017; accepted in final form 11 July 2017

Strangman GE, Ivkovic V, Zhang Q. Wearable brain imaging with multimodal physiological monitoring. *J Appl Physiol* 124: 564–572, 2018. First published July 13, 2017; doi:10.1152/japplphysiol.00297.2017.—The brain is a central component of cognitive and physical human performance. Measures, including functional brain activation, cerebral perfusion, cerebral oxygenation, evoked electrical responses, and resting hemodynamic and electrical activity are all related to, or can predict, health status or performance decrements. However, measuring brain physiology typically requires large, stationary machines that are not suitable for mobile or self-monitoring. Moreover, when individuals are ambulatory, systemic physiological fluctuations—e.g., in heart rate, blood pressure, skin perfusion, and more—can interfere with noninvasive brain measurements. In efforts to address the physiological monitoring and performance assessment needs for astronauts during spaceflight, we have developed easy-to-use, wearable prototypes, such as NINscan, for near-infrared scanning, which can collect synchronized multimodal physiology data, including hemodynamic deep-tissue imaging (including brain and muscles), electroencephalography, electrocardiography, electromyography, electrooculography, accelerometry, gyroscopy, pressure, respiration, and temperature measurements. Given their self-contained and portable nature, these devices can be deployed in a much broader range of settings—including austere environments—thereby, enabling a wider range of novel medical and research physiology applications. We review these, including high-altitude assessments, self-deployable multimodal e.g., (polysomnographic) recordings in remote or low-resource environments, fluid shifts in variable-gravity, or spaceflight analog environments, intracranial brain motion during high-impact sports, and long-duration monitoring for clinical symptom-capture in various clinical conditions. In addition to further enhancing sensitivity and miniaturization, advanced computational algorithms could help support real-time feedback and alerts regarding performance and health.

ambulatory brain imaging; diffuse optical tomography; near-infrared spectroscopy; physiological monitoring

INTRODUCTION

Advances in sensors, microelectronics, and computational capabilities have resulted in a recent explosion of wearable sensing technologies. These technologies can provide physiological measurements in volunteers or patients, as they go about their ordinary daily activities, or even during vigorous motion (1, 28, 47, 51). Ambulatory monitoring for the brain, however, has lagged behind the now-commonplace accelerometry and cardiac sensors. Beyond ambulatory EEG, which is predominantly used for seizure detection and quantification (27), only a handful of wearable systems for brain monitoring exist, based on near-infrared spectroscopy (NIRS) (35). Only two such wearable NIRS devices support imaging, and none of these support simultaneous multimodal physiological recording.

Obtaining valid and interpretable measurements of brain function in active persons or in austere environments poses numerous challenges. Active subjects generate motion artifacts, changes in blood pressure, heart rate, skin temperature and perfusion, among other variables. Ambulatory individuals also experience significant environmental changes, such as electromagnetic interference, extreme changes in ambient lighting or temperature, vibrations, and other conditions. Because it is generally not possible to control such variables, mobile brain imaging systems need to measure them. Ideally, mobile brain monitoring systems would also be sufficiently stable and sensitive to enable long-duration monitoring (over many hours) to help bridge multiple temporal scales, ranging from milliseconds to far beyond the typical 1- or 2-h neuro-

Address for reprint requests and other correspondence: G. Strangman, Neural Systems Group, MGH, Bldg. 149, 13th St., Rm. 10.028, Charlestown, MA 02129 (e-mail: strang@nmr.mgh.harvard.edu).

imaging session. Having encountered the above issues when trying to monitor active and remote subjects, we began developing prototype technologies to target mobile and real-time brain monitoring and imaging along with simultaneous multiparameter physiological monitoring.

The purpose of this paper is to review our progress in multimodal ambulatory brain and physiological monitoring. Initial prototypes (55, 56) recorded up to four NIRS channels, typically with one short and one long source detector (SD) separation to measure superficial and deep tissue hemodynamics, respectively (41). These prototypes also included accelerometry to measure head motion independent of NIRS, plus ECG for heart rate and waveform analysis. More recent prototypes (15) add NIRS channels to enable three-dimensional (3D) tomographic imaging, while also expanding the physiological and auxiliary recording capabilities. Miniaturization is an ongoing effort, with a goal of fully plug-and-play physiological sensing coupled with whole head continuous, ambulatory brain imaging. We describe the advantages, provide example applications, and show the limitations of our current prototypes, as well as future possibilities for such technologies.

MATERIALS AND METHODS

The NINscan prototypes are self-contained, multimodal physiological recording systems currently supporting up to 64-channel, 16-bit continuous-wave NIRS and diffuse optical tomography (DOT) brain imaging capabilities. Current systems (<500 cm^3 and <0.5 kg) were designed for mobility and flexibility, including continuous recording for more than 24 h on four rechargeable AA batteries. The NIRS subcomponent currently uses up to four dual-wavelength laser diode sources (780/830 nm; Axcel Photonics, Marlborough, MA) and up to eight photodiode detectors (OPT101; Texas Instruments, Dallas, TX) for ambulatory DOT. As such, they can perform regional imaging of oxy-hemoglobin (O_2Hb), deoxy-hemoglobin (HHb), and total hemoglobin (HbT) concentrations (39). The device's optical elements are deployable in user-defined geometries for head/brain, limb, abdominal, or multisite applications. Automatic, multistage gain control supports 300,000-fold amplification (for a >125-dB system dynamic range), with gain settings determined automatically when the instrument is powered on, and switched dynamically during device operation. This design can accommodate detectors that are positioned close to a light source (e.g., ~1 cm) for measuring fat or skin layer physiology, and far from light sources for deeper tissue measurements (10, 23, 41, 42, 53, 54). The maximum achievable SD separation—and, hence, depth sensitivity (41)—depends on many factors, but SD separations of 40–50 mm have regularly been achieved.

In parallel, NINscan-M supports *1*) up to 8 gain-controllable 24-bit analog inputs compatible with ECG, EMG, EOG, EEG, or other biopotential or analog signal sources, *2*) up to another six 12-bit analog input channels, and *3*) up to six digital sensor inputs, all sampled at up to 250 Hz. The 24-bit analog inputs are supported by a low-noise analog front-end (ADS1299; Texas Instruments) to enable recording of microvolt-level EEGs. The 12-bit analog inputs have been used to support both pressure and respiration-induced plethysmography (RIP) sensors. Through the digital inputs, we have integrated high- and low-range accelerometers, gyroscopes, and temperature sensors. Additional digital-in or -out lines are available for synchronizing with other stimulus or recording devices, and four user-input buttons provide a method for marking external events directly in the data stream, at the underlying 4-ms temporal resolution.

Device deployment was designed to minimize training needs. Users need only position the sensors and turn the system on; configuration is completed automatically. When recording, the CPU continuously stores all data on an SD flash memory card; a 32-Gb card can store >200 h of continuous recording. The device can be turned off at any time and restarted as needed (each new recording is saved to newly time-stamped file). Data transfer is achieved via the SD card, and the system can be configured for real-time Bluetooth broadcast of acquired data by setting configuration parameters in a simple text file.

The NIRS sensor pads are designed for low-profile and highly motion-robust use, as in our previous designs (56). A lightweight, flexible form holds the laser diodes and photodiodes. A medical tape layer is used for interfacing, and light shaping diffusers are attached to the surface of the laser diodes to broaden the source beam. In some applications, we affix small (3×5 mm) coated lenses (Edmunds Optics) to the optical components to improve coupling, particularly for applications through thick hair on the head. The portions of the sensor that contact the subject are, thus, either glass, polycarbonate, medical tape, or nylon, to maximize biocompatibility. Being prototypes, the NINscan systems are not FDA-approved.

NINscan-SE is a customized version specifically targeting sleep and EEG research. This system has a separate ground for ECG to minimize ECG artifacts in the lower-amplitude EEG, EOG and EMG channels. It also incorporates an input for a commercial respiratory induction plethysmography (Pro-Tech zRIP, Philips) to monitor respiratory volume. Figure 1*A* shows our most recent NINscan-SE monitor, including the recording box (150×75 mm), an example 64-channel NIRS imaging probe, biopotential leads for ECG/EMG/EOG/EEG, and the other sensors that we have, thus far, integrated (respiration, accelerometer, gyroscope, temperature, and force).

EXAMPLE APPLICATIONS IN PHYSIOLOGY

Our multimodal prototypes have previously been deployed *1*) to gather brain, cardiac, and accelerometry data during parabolic flight and high-altitude hiking (56), *2*) in 24-h continuous ambulatory monitoring during activities of daily living including sleep, eating, driving, and playing sports (55), as well as *3*) for muscle oxygenation and physiological monitoring during a variety of exercise applications, including isometric flexions, cycling, and free running (15). Below, we summarize these and other examples made possible by the NINscan prototypes.

Three-dimensional wearable brain imaging. Our key goal has been to enable wearable 3D DOT imaging of functional brain activity alongside multiparameter physiological monitoring. We tested the imaging system with a 100×40-mm array positioned over left dorsolateral prefrontal cortex (Fig. 1*C*) during a block-design N-back working memory task (24) with six 22-s active periods interleaved with 22-s rest periods. After block-averaging, HHb concentrations were reconstructed at multiple depths in tissue using a linear image reconstruction algorithm: Rytov approximation and semi-infinite boundary condition for forward modeling, and inverse modeling using a truncated singular value decomposition technique (15, 34, 50). As found in previous functional MRI and PET investigations of the N-back task (4, 19, 33), functional activation evidenced by significant but focal decreases in HHb concentrations (and increases in O_2Hb)—consequent to focal blood flow increases from neurovascular coupling (45)—were observed, primarily at depths corresponding to the outer 10 mm of brain tissue. This highlights the importance of the auto-gain and multidistance capabilities of the NIRS sensor components, which support the ability to conduct regional deep tissue tomographic imaging. The same NIRS imaging sensor has also been used to image muscle oxygenation changes during active motor and exercise tasks (15). The observed sensitivity (in terms of SD separations) compares favorably with existing mobile systems

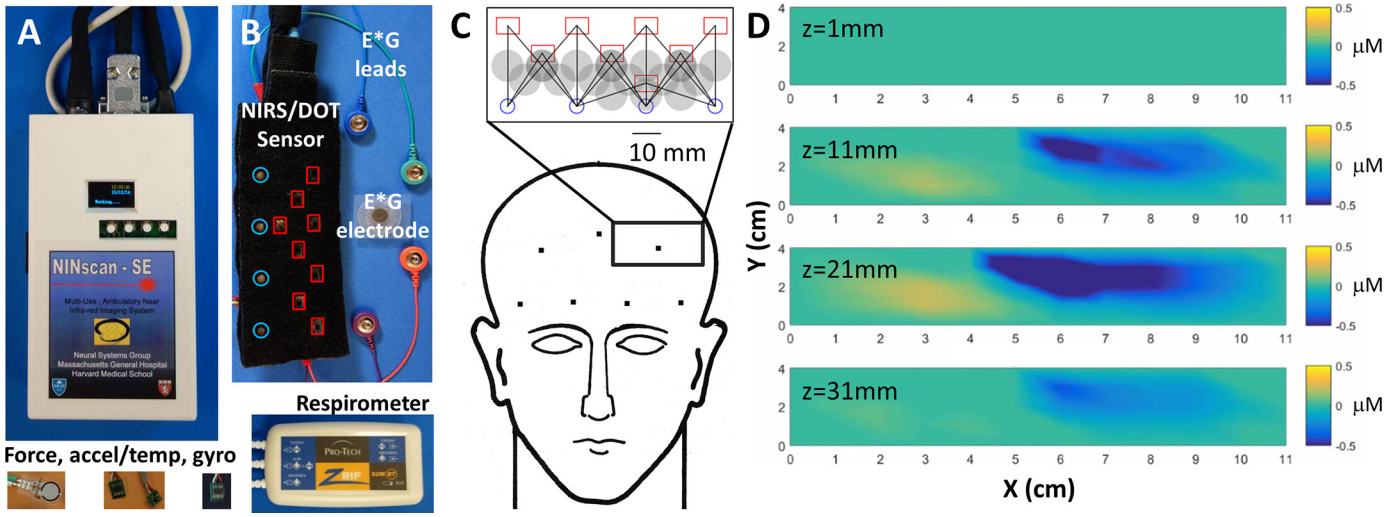

Fig. 1. NINscan brain imaging. *A*: NINscan-SE recorder with OLED screen and four user buttons. *B*: 64-channel near-infrared spectroscopy (NIRS) sensor enables three-dimensional diffuse optical tomography (blue circles denote laser diodes, while red rectangles denote photodetectors), whereas standard ECG leads and electrodes support 8-channel biopotential monitoring. Additional sensors include force, acceleration, temperature, gyroscopy, and respiration (up to 81 channels in all; photos are to scale). *C*: illustration of DOT probe and positioning over F3 (left dorsolateral prefrontal cortex) for functional NIRS of an N-back task. *D*: reconstructed deoxy-Hb concentrations at multiple layers in depth from the surface of the head, illustrating functional activation (deoxy-Hb decreases; unpublished findings, Strangman GE, Ivkovic V) associated with 2-back task performance (19).

and even many current, immobile, laboratory-based NIRS-imaging devices.

Physiological brain responses at high altitude. A unique capability afforded by the wearable NINscan technology is deployment in remote and extreme environments. One example test was conducted during a multiday high-altitude hike up Mt. Kilimanjaro, with recordings collected both during hiking (56), as well as at the end of each day (at different altitudes) during various physiological challenges. Figure 2*A* shows the use of a four-channel NINscan collecting NIRS, ECG, and accelerometry data at Uhuru peak (5,895 m). Figure 2*B* shows hemodynamic responses to repeated Valsalva (*top*) and Mueller (*bottom*) maneuvers in both brain and overlying scalp tissue under hypoxic conditions. This highlights the feasibility of self-deployment in remote and low-resource settings to monitor brain oxygenation, the repeatability and low-noise of such recordings, as well as unexpectedly larger brain responses to these challenges than the simultaneously measured overlying scalp tissue.

Long-duration, self-deployed sleep polysomnography. In addition to remotely deployed monitoring, we also sought to support unobtrusive, long-duration applications in low-resource settings. NINscan-SE was developed for NASA specifically to enable spaceflight-compatible, self-deployed sleep polysomnography (PSG). This system includes a 64-channel DOT sensor for hemodynamic imaging across the forehead (spanning F3 to F4), plus configuration of the eight biopotential inputs into 3-channel EEG (F3, Fz, F4), 2-channel EOG, 2-channel EMG, 1-channel ECG, accelerometry, RIP respirometry, and skin temperature sensing (cf. Fig. 1, *A* and *B*). Such multiparameter data are essential for reliable PSG evaluation. The goal of this effort was to obtain robust, objective multiday sleep data on volunteers participating in 30-day isolation missions in NASA's Human Exploration Research Analog (Fig. 2, *C* and *D*). These missions allowed less than 60 min of training on how and where to place the sensors and system operation, and no sleep or hardware technicians were available during data collection. Eight participants were sequestered for 30 days, and the NINscan-SE was deployed for its PSG capabilities on five nights/participant during the mission. Multimodal data from the eight distinct sensor types (EEG, EOG, EMG, ECG, temperature, respiration, accelerometry, and NIRS) were converted to standard PSG data formats (European Data Exchange, or EDF) to support review and analysis in standard PSG software packages (Fig. 2*D*).

The key test was whether the system, deployed in this manner, could generate sufficiently reliable data for sleep scoring using the American Academy of Sleep Medicine standard (3). Some 98.7 ± 1.2% of the 30-s epochs exhibited sufficiently high-quality data for scoring (on par with technician-led sleep recordings; Fig. 2*D*), and the resulting hypnograms provided sleep staging consistent with sleep records from healthy subjects undergoing inpatient sleep testing (12). This included a total sleep time of 6.5 ± 1.5 h, sleep latency of 36 ± 25 min, Stage R latency of 112 ± 43 min, first wake after sleep onset at 33 ± 31 min, sleep efficiency of 85 ± 8%, and staging N1 = 11%, N2 = 54%, N3 = 14%, and rapid eye movement (REM) = 21%. While clinical validation remains to be completed, such work demonstrated that even with limited training and unmonitored self-deployment, NINscan-SE provided reliable, long-duration, and multimodal physiological data and quantitative sleep metrics in isolated, low-resource settings. A key feature was, of course, the ability to collect multimodal physiological data to identify artifacts, differentiate REM from NREM, wake from sleep, and so forth.

Simulated microgravity effects on brain-blood volume and hemodynamics. A current concern of NASA is known as spaceflight-associated neuro-ophthalmological syndrome (SANS), in which some astronauts in flight begin to exhibit posterior flattening of the eye orbit, choroidal folds, and, in some cases, optic nerve sheath swelling (26). This condition has an unknown etiology, but cephalad fluid shifts (2, 48) are

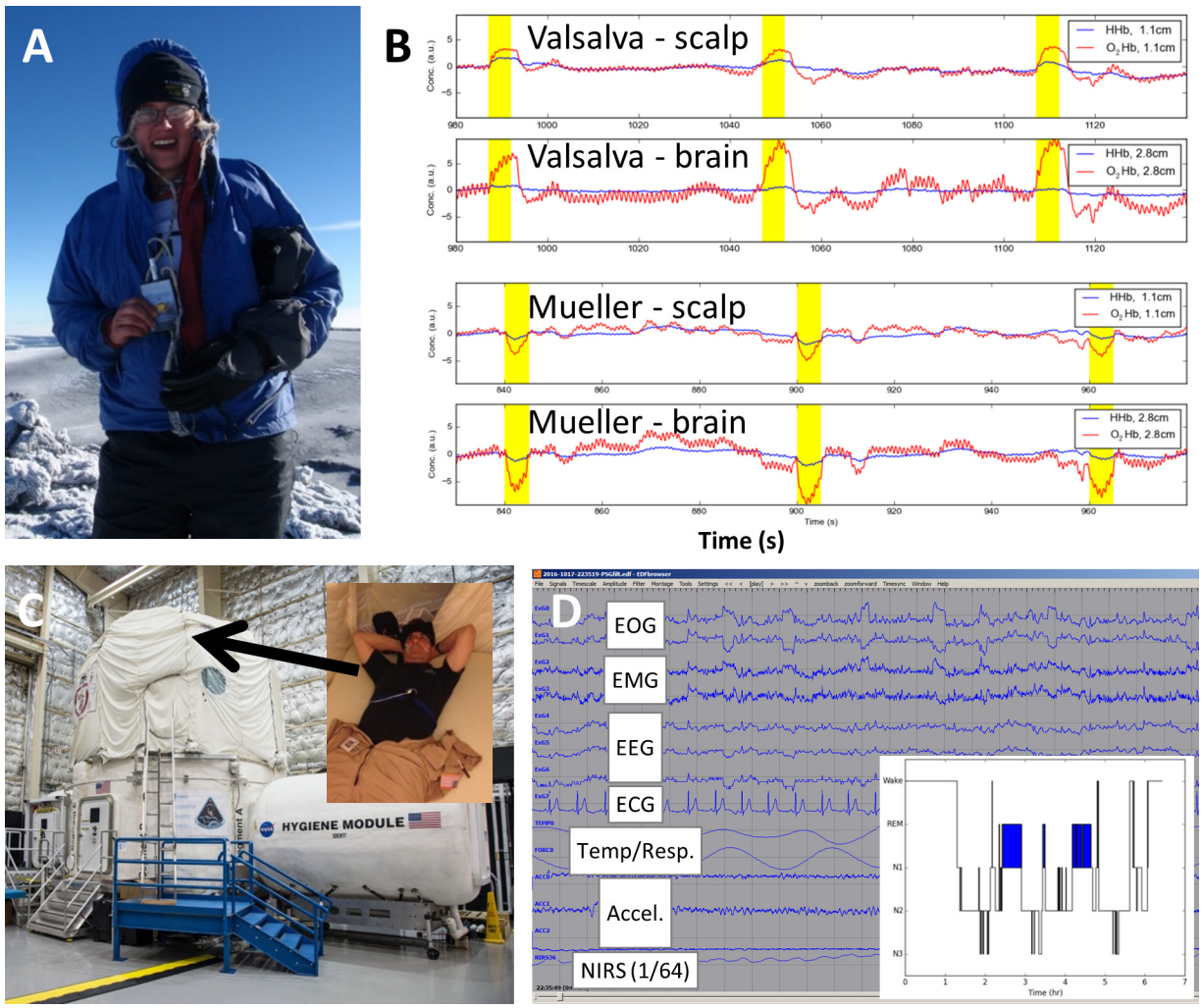

Fig. 2. Remote and long-duration brain monitoring. *A*: NINscan being deployed during high-altitude hiking atop Mt. Kilimanjaro (56). *B*: example systemic and brain oxygenation responses to Valsalva and Mueller maneuvers collected at 4,800 m altitude (unpublished findings, Williams E, Patz S, Zhang Q, Strangman GE). *C*: NASA's Human Exploration Research Analog has been used for testing self-deployed multi-channel PSG during 30-day isolation studies. *D*: NINscan-SE PSG recordings were of sufficient quality for hypnogram scoring via the American Academy of Sleep Medicine standard (*inset*).

currently thought to be contributing factors (52). Intracranial blood distribution changes are also highly relevant to syncope (44) and orthostatic intolerance (2, 17). We used a progressive head-down tilt (HDT) protocol to induce cephalad fluid shifts (13) coupled with a four-arm sensor for NINscan-M to monitor regional tissue [HbT] at multiple points along the body axis—a capability that typically requires multiple NIRS systems (Fig. 3, *A* and *B*). NINscan simultaneously monitored tilt via accelerometer, as well as skin temperature as a NIRS covariate.

Healthy volunteers ($n = 8$) were sequentially positioned in $+50°$ head-up tilt (HUT), $0°$ (supine), and $-6°$ HDT orientations for 20 min each. Progressively reducing G_z led to significantly increased [HbT] in prefrontal cortex (mixed effects linear regression: $z = -2.58$, $P = 0.02$). The effect was nonlinear with tilt in that brain [HbT] increased as much between $+50°$ to $0°$ as it did from $0°$ to $-6°$. A similar finding was observed for the gastrocnemius muscle, but in the opposite direction, such that decreasing HDT tilt led to significant and progressive decreases in leg [HbT] ($z = 3.01$; $P = 0.003$). While [HbT] is not a direct measure of regional blood volume, it is generally proportional to tissue blood volume assuming constant hematocrit during the 60-min recording. The synchronized measures, along with accelerometry to confirm both tilt and head stability are, thus, being used to help quantify hemodynamic shifts as a function of tilt angle, as well as investigating potential countermeasures to mitigate such fluid shifts.

While HDT provides one analog of spaceflight-relevant fluid shifts, another relevant analog is parabolic flight, which generates up to ~20-s periods of microgravity during each parabolic descent. We deployed four-channel, flight-compatible NINscan sensors over lateral prefrontal cortex, along with accelerometry and ECG, on seated individuals during 10 parabolas. Brain oxygenation and hemodynamics were calculated using the modified Beer-Lambert law (8) and block-averaged, triggered on the onset of microgravity. Extracranially, we found reliable increases in all hemoglobin species, including a ~10-μM increase in [HbT]. Intracranially, the [HbT] increase was smaller, suggesting that autoregulation mechanisms may help maintain equilibrium cerebral fluid volumes (Fig. 3*C*). Unlike extracranial tissues, an increase in intracranial [O_2Hb] was coupled with a concomitant decrease in [HHb]. This is a

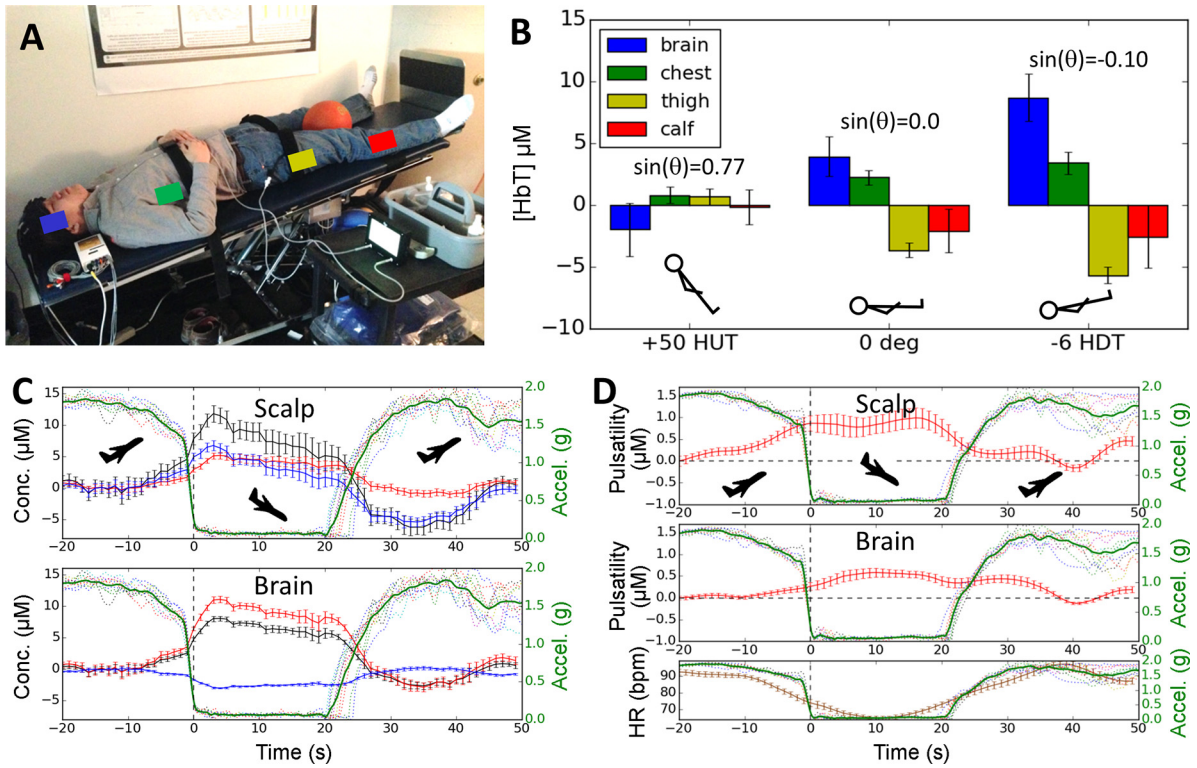

Fig. 3. Spaceflight-relevant cerebral fluid shifts. *A*: NINscan-M deployed during −6° head-down tilt with sensors on lateral head, chest, thigh, and calf (colors) to measure whole body fluid shifts. *B*: [HbT] at each measurement position in *A* as a function of body orientation, relative to +70° head-up tilt (HUT; $n = 8$; means ± SE). Significant increases in [HbT] were observed in the head with progressive HDT, alongside significant [HbT] decreases in the leg, helping to quantify the extent and regional specificity of fluid shifts with HDT. *C*: extracranial (scalp) and intracranial (brain) [O_2Hb], [HHb], and [HbT] in an example subject during parabolic flight (56); see text. Right axis corresponds to accelerometry trace (green). *D*: cardiac pulsatility in [HbT] increases in both scalp and brain tissues during the same parabolic flight, while heart rate decreases associated with microgravity (unpublished findings, Ivkovic V, DiPasquale D, Zhang Q, Strangman GE).

prototypical pattern seen in functional brain activation (20, 40) and indirectly suggests an increase in blood flow to the brain. In this case, however, the magnitude of the hemoglobin changes is roughly 10-fold greater than a typical functional NIRS response from prefrontal cortex.

Given NINscan's 25-Hz temporal resolution, we also measured the amplitude of cardiac pulsatility in [HbT] (i.e., vasculature volume changes) during the flight (43). Pulsatility significantly increased both in the scalp and, to a lesser extent, in brain tissue (Fig. 3*D*). In parallel, ECG revealed a nearly 20-bpm decrease in heart rate during the microgravity period. Although we did not simultaneously measure intracranial pressure, we have previously suggested that increased [HbT] pulsatility inside the skull could be associated with increased vascular distention and dynamic (peak-to-peak) intracranial pressure pulsatility (43). Changes in heart rate along with increased cerebral pulsatility and increased cerebral blood flow could all potentially play a role in SANS symptoms from microgravity exposure.

Head movement and impact on brain motion. Concussions and traumatic brain injury (TBI) are important medical concerns in military, sports, and trauma medicine. Sudden accelerations and decelerations are known to cause the brain to move toward or away from the inner skull surface, but the evidence is typically indirect because monitoring brain motion in healthy human subjects is difficult. NIRS is known to exhibit an exponential sensitivity gradient as a function of depth in tissue (41, 42). Although this is often considered a weakness of NIRS—limiting sensitivity to deeper tissues—we exploited this characteristic by investigating whether NIRS could detect movement of the brain within the skull during periods of rapid acceleration and deceleration in freely moving subjects. Assuming a motion-robust NIRS system, one would predict detectable increases in [HbT] as the brain moves closer to the sensor and skull (41).

In Fig. 4*A*, glass-brain MRI images illustrate rapidly moving one's head left and right (shaking "no"). As the head moves, the brain is assumed to alternately move toward and away from the skull, in an anti-phase manner between left and right sides of the head. To test this hypothesis, we used NINscan-M to record from four near-orthogonal points on the head—F3, F4, Fz, and Cz in the International 10–20 system (14, 38); see Fig. 4*A*, *top*—while subjects rapidly shook their head back and forth and NINscan-M's gyroscope simultaneously quantified head motion (Fig. 4*B*). The left and right NIRS sensors exhibited oscillatory, anti-phase [HbT] changes associated with the rotational motion as predicted (vertical arrow, Fig. 4*C*). Frontal and superior locations exhibited more complex relationships to the gyroscope measurements, perhaps given their positions on the head and the predominantly yawing rotational head motion. Importantly, the NIRS data were corrected via a colocated measurement of superficial layer interference (32). This suggests the observed changes are not systemic or motion artifacts, but instead reflect brain motion within the skull.

We used this same approach to monitor football players during realistic tackling drills, as illustrated in Fig. 4*D*. The

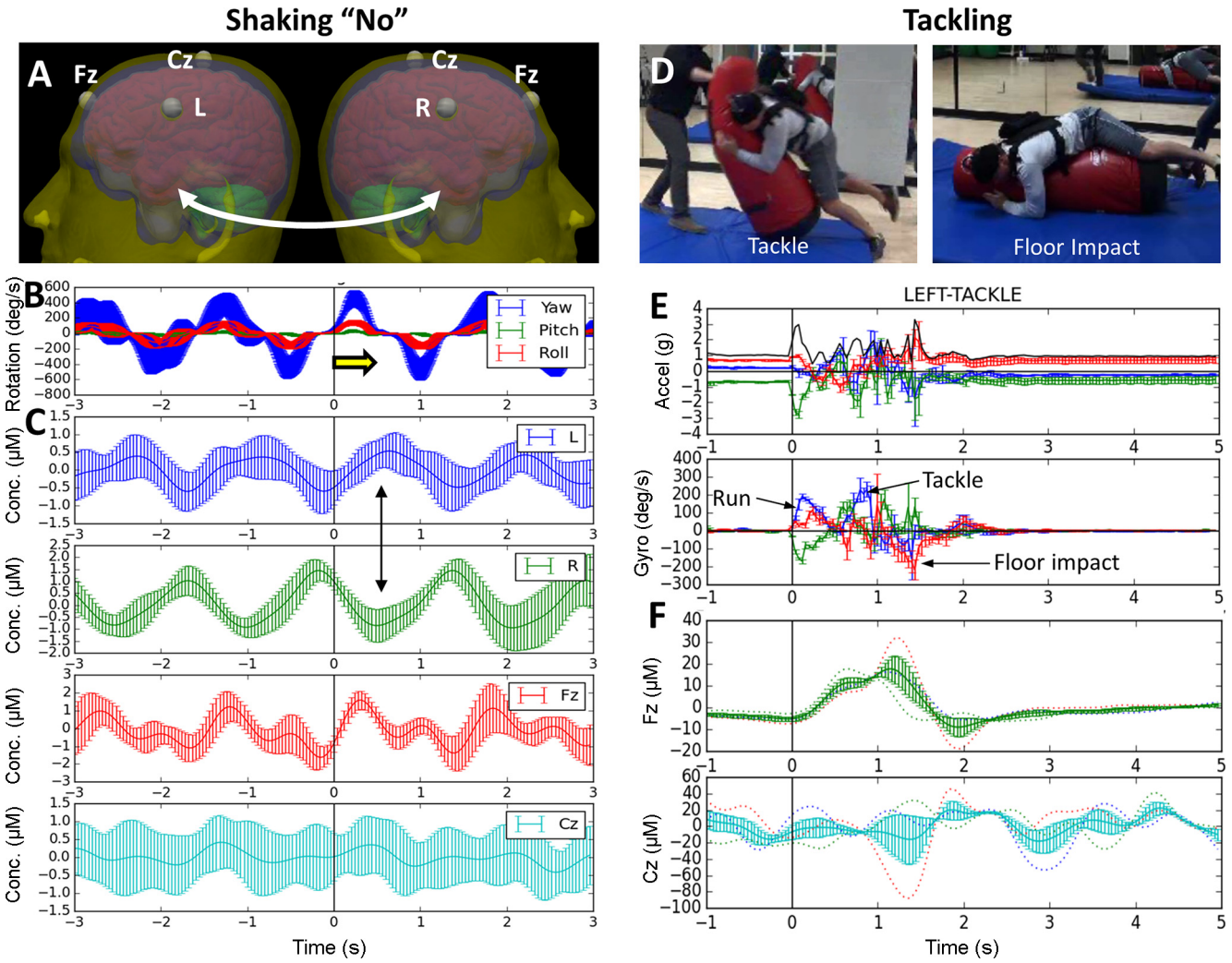

Fig. 4. Brain motion detection. *A*: Glass-brain illustration of shaking one's head left and right, with the locations of four NINscan-M sensors (F3, F4, Fz, and Cz), plus accelerometry and gyroscope monitoring. *B*: average gyroscope output, triggered on turning the head to the right (yellow arrow). *C*: brain [HbT] responses synchronized to the gyroscope, illustrating antisymmetric fluctuations from left and right sensors (vertical arrow) and more complex responses from Fz and Cz. *D*: photos of the tackling protocol while wearing NINscan-M. *E*: accelerometer and gyroscope responses averaged over three trials (means ± SE) during tackling maneuver. *F*: The [HbT] increase at Fz during the tackle is consistent across trials, and an order of magnitude larger than the changes observed in *C* (unpublished findings, Ivkovic V, Zhang Q, Strangman GE).

two panels in Fig. 4*E* show the complex but reproducible accelerometry and gyroscope profiles over three separate trials by a single subject performing a tackling drill: three-point stance, rise, run 2 steps, grab dummy, and tackle it to the floor. The two panels in Fig. 4*F* show the response of the brain in frontal and superior locations, with a dramatic increase in [HbT] detected at Fz during tackle decelerations. This frontal change is ~10-fold larger than shaking the head back and forth (Fig. 4*B*), providing initial quantitative information about the extent of tissue movement within the head during ordinary motion vs. higher-impact activities. Such work suggests that NINscan is sufficiently motion-robust to be used in high-impact settings, and the synchronized gyroscope data help quantify the direction and magnitude of brain motion inside the skull.

DISCUSSION

The primary distinguishing characteristic of our NINscan prototypes is the ability to combine continuous, long-duration, and ambulatory hemodynamic brain imaging with multimodal physiological monitoring—in an easily deployed, self-contained package. Our examples demonstrate that this approach enables brain imaging in new ways, new places, and more frequent monitoring, including continuous monitoring. Suitable domains beyond those demonstrated here include those in which neurological or psychiatric symptoms or events occur infrequently and semirandomly (i.e., not on-demand while at the hospital). Syncope is one example, where portable cerebral oxygenation and perfusion measures alongside ECG, accelerometry, and ambulatory blood pressure are key to detecting, characterizing, and helping predict syncopal and presyncopal episodes. Other relevant conditions with intermittent or unpredictable symptomatology include *1*) epilepsy, *2*) cerebrovascular accidents following stroke or cardiovascular or neurosurgical procedures, and *3*) continuous stroke or cerebral autoregulation monitoring (21), as well as monitoring for effects of anesthesia, sudden infant death syndrome, and sleep-disordered breathing. So, while wearable accelerometers enable fall

detection (57), and wearable ECG enables cardiac arrhythmia detection (18), our approach enables investigation, monitoring, and quantification of conditions with infrequent and unpredictable cerebral hemodynamic symptoms.

A second broad category of investigations made possible are those requiring remote or point-of-care brain assessments. Examples from our work include *1*) parabolic flight (56), *2*) activities at high-altitude (56), *3*) brain monitoring during football drills, and *4*) sequestration studies. Our results clearly demonstrate the possibility of investigating other high-impact sports (e.g., hockey, soccer, and cycling), sidelines assessment of brain hemodynamics postinjury during sporting events (e.g., to support return-to-play decisions), on-site trauma or stroke assessment, investigation of cerebral (or muscle) factors in fatigue during exercise (5, 30, 36, 46), or more general brain and physiology monitoring in realistic contexts like driving a car, flying an airplane, first-responder training, rural/remote settings, or military applications. All of these cases represent situations in which standard neuroimaging technologies (MRI, PET, CT) are infeasible—for reasons of portability, mobility, cost, and/or restrictions on serial imaging due to radiation exposure limits.

A third category of applications involve prediction. The vast majority of brain imaging research focuses on the results from one or two snapshot measurements of brain activity. In contrast, long-duration monitoring capabilities provide key temporal information on physiological responses. Applications include, among others, monitoring neurophysiological effects of medications, radiation exposure, or cognitive therapies over hours or days. Such serial imaging can improve our understanding of cerebral and physiological variables over time, which, in turn, supports prediction—and potentially even online optimization—of performance (22). That is, given a detailed understanding of baseline fluctuations, one can endow on-board microprocessors with algorithms to support real-time detection and decision making. This could range from algorithms to alert a patient of an imminent syncopal episode to help prevent injury, similar to ambulatory EEG-based seizure-alerting algorithms (6), to performance optimization in elite athletes.

Vital to all of the above applications is multimodal data collection. Accelerometers and gyroscopes quantify motion and can be used for artifact detection in all channels (7). Skin temperature and close SD pairs are relevant covariates for NIRS (25, 31). EOG and EMG can provide important physiological data (e.g., for PSG sleep scoring) and also support artifact rejection in EEG (16). ECG can be used for NIRS noise suppression (11), to generate heart rate covariates, or even for continuous blood pressure measurement (29). Thus, the synergies of the multimodal approach enable a much more comprehensive understanding of the individual's state, physiological covariates, and potential confounding factors in the data and enables more robust data interpretation.

Our prototype devices continue to evolve in terms of miniaturization, computing power and measurement capabilities. Although systems currently have a maximum of 64 NIRS channels, we are investigating designs for high-density DOT (9) that include over 1,000 NIRS channels, while still remaining fully wearable and motion-robust. Traditional NIRS detectors can also be replaced with novel nonlinear optical components (49) or flexible optoelectronics (37) to improve depth and spatial sensitivity, while simultaneously enhancing wearability. Similarly, the current maximum of eight biopotential channels could be expanded to provide higher density (yet still mobile) EEG, 12-lead ECG, or other multisite biopotential monitoring. Additional auxiliary sensors could also be supported, including blood pressure and electrodermal responses.

Important limitations still need to be overcome. In particular, all mobile NIRS devices have relatively few channels, which limits spatial resolution and spatial coverage for brain imaging. NIRS also has limitations in terms of penetration depth into tissue. These two limitations can be addressed by deploying more sources and detectors, more sensitive detectors and lowering detector and system noise floors. In addition, our current set of auxiliary sensors is still modest. And, real-time prediction applications will require substantial work first to understand normal baseline physiological fluctuations, and then develop the algorithms that identify key parameters and generate predictions with sufficiently low false-positive and false-negative alerts. Finally, while the sensitivity and robustness of NINscan systems have been demonstrated in a wide range of conditions, we have yet to conduct head-to-head comparisons against commercial laboratory devices measuring each of the individual variables.

Despite these limitations, however, the combination of ambulatory brain imaging plus multimodal physiology affords many new opportunities. To date, brain monitoring and imaging have been largely restricted to snapshots taken in confining machines located in major neuroimaging centers. Our goal has been to eliminate as many barriers as possible—obtrusiveness, robustness, complexity, and cost—and enable brain monitoring in settings where brain assessment was previously considered impossible. Doing so fundamentally requires a multimodality approach—so that brain imaging data can be properly interpreted given the wide variety of physiological and environmental changes that can occur in home, ambulatory, remote, or even extreme settings outside the traditional neuroimaging center.

ACKNOWLEDGMENTS

We acknowledge the hardware and firmware development expertise of Dr. Gang Hu and further support from Ning Zhang, Erika Williams, and Team Uhuru for high-altitude hiking data; the NASA Flight Analogs Program for experimental support in parabolic flight and HERA; and Brandon Lockyer for polysomnographic expertise.

GRANTS

This work was supported by the National Space Biomedical Research Institute through NASA NCC 9-58 and the National Football League Players Association (NFLPA). The content is solely the responsibility of the authors and does not necessarily represent the official views of the NFLPA, Harvard University or Massachusetts General Hospital.

DISCLOSURES

Drs. Zhang and Strangman jointly hold one patent and one patent application related to mobile brain imaging. No licenses have been granted for either.

AUTHOR CONTRIBUTIONS

G.E.S., V.I., and Q.Z. conceived and designed research; G.E.S., V.I., and Q.Z. performed experiments; G.E.S., V.I., and Q.Z. analyzed data; G.E.S., V.I., and Q.Z. interpreted results of experiments; G.E.S. and V.I. prepared figures; G.E.S. drafted manuscript; G.E.S., V.I., and Q.Z. edited and revised manuscript; G.E.S., V.I., and Q.Z. approved final version of manuscript.

REFERENCES

1. **Altini M, Casale P, Penders J, Ten Velde G, Plasqui G, Amft O.** Cardiorespiratory fitness estimation using wearable sensors: laboratory and free-living analysis of context-specific submaximal heart rates. *J Appl Physiol (1985)* 120: 1082–1096, 2016. doi:10.1152/japplphysiol.00519.2015.
2. **Baisch F, Beck L, Blomqvist G, Wolfram G, Drescher J, Rome JL, Drummer C.** Cardiovascular response to lower body negative pressure stimulation before, during, and after space flight. *Eur J Clin Invest* 30: 1055–1065, 2000. doi:10.1046/j.1365-2362.2000.00750.x.
3. **Berry RB, Brooks R, Gamaldo CE, Harding SM, Lloyd RM, Marcus CL, Vaughn BV.** *The AASM Manual for the Scoring of Sleep and Associated Events: Rules, Terminology and Technical Specifications*. Darien, IL: American Academy of Sleep Medicine, 2015.
4. **Carlson S, Martinkauppi S, Rämä P, Salli E, Korvenoja A, Aronen HJ.** Distribution of cortical activation during visuospatial n-back tasks as revealed by functional magnetic resonance imaging. *Cereb Cortex* 8: 743–752, 1998. doi:10.1093/cercor/8.8.743.
5. **Carroll TJ, Taylor JL, Gandevia SC.** Recovery of central and peripheral neuromuscular fatigue after exercise. *J Appl Physiol (1985)* 122: 1068–1076, 2017. doi:10.1152/japplphysiol.00775.2016.
6. **Cogan D, Birjandtalab J, Nourani M, Harvey J, Nagaraddi V.** Multi-biosignal analysis for epileptic seizure monitoring. *Int J Neural Syst* 27: 1650031, 2017. doi:10.1142/S0129065716500313.
7. **Cooper RJ, Selb J, Gagnon L, Phillip D, Schytz HW, Iversen HK, Ashina M, Boas DA.** A systematic comparison of motion artifact correction techniques for functional near-infrared spectroscopy. *Front Neurosci* 6: 147, 2012. doi:10.3389/fnins.2012.00147.
8. **Cope M, Delpy DT, Reynolds EOR, Wray S, Wyatt J, van der Zee P.** Methods of quantitating cerebral near infrared spectroscopy data. *Adv Exp Med Biol* 222: 183–189, 1988. doi:10.1007/978-1-4615-9510-6_21.
9. **Eggebrecht AT, Ferradal SL, Robichaux-Viehoever A, Hassanpour MS, Dehghani H, Snyder AZ, Hershey T, Culver JP.** Mapping distributed brain function and networks with diffuse optical tomography. *Nat Photonics* 8: 448–454, 2014. doi:10.1038/nphoton.2014.107.
10. **Funane T, Sato H, Yahata N, Takizawa R, Nishimura Y, Kinoshita A, Katura T, Atsumori H, Fukuda M, Kasai K, Koizumi H, Kiguchi M.** Concurrent fNIRS-fMRI measurement to validate a method for separating deep and shallow fNIRS signals by using multidistance optodes. *Neurophotonics* 2: 015003, 2015. doi:10.1117/1.NPh.2.1.015003.
11. **Gratton G, Corballis PM.** Removing the heart from the brain: compensation for the pulse artifact in the photon migration signal. *Psychophysiology* 32: 292–299, 1995. doi:10.1111/j.1469-8986.1995.tb02958.x.
12. **Grigg-Damberger MM.** The AASM Scoring Manual four years later. *J Clin Sleep Med* 8: 323–332, 2012. doi:10.5664/jcsm.1928.
13. **Hargens AR, Vico L.** Long-duration bed rest as an analog to microgravity. *J Appl Physiol (1985)* 120: 891–903, 2016. doi:10.1152/japplphysiol.00935.2015.
14. **Homan RW, Herman J, Purdy P.** Cerebral location of international 10-20 system electrode placement. *Electroencephalogr Clin Neurophysiol* 66: 376–382, 1987. doi:10.1016/0013-4694(87)90206-9.
15. **Hu G, Zhang Q, Ivkovic V, Strangman GE.** Ambulatory diffuse optical tomography and multimodality physiological monitoring system for muscle and exercise applications. *J Biomed Opt* 21: 091314, 2016. doi:10.1117/1.JBO.21.9.091314.
16. **Islam MK, Rastegarnia A, Yang Z.** Methods for artifact detection and removal from scalp EEG: A review. *Neurophysiol Clin* 46: 287–305, 2016. doi:10.1016/j.neucli.2016.07.002.
17. **Iwasaki K, Levine BD, Zhang R, Zuckerman JH, Pawelczyk JA, Diedrich A, Ertl AC, Cox JF, Cooke WH, Giller CA, Ray CA, Lane LD, Buckey JC Jr, Baisch FJ, Eckberg DL, Robertson D, Biaggioni I, Blomqvist CG.** Human cerebral autoregulation before, during and after spaceflight. *J Physiol* 579: 799–810, 2007. doi:10.1113/jphysiol.2006.119636.
18. **Jager F, Taddei A, Moody GB, Emdin M, Antolic G, Dorn R, Smrdel A, Marchesi C, Mark RG.** Long-term ST database: a reference for the development and evaluation of automated ischaemia detectors and for the study of the dynamics of myocardial ischaemia. *Med Biol Eng Comput* 41: 172–182, 2003. doi:10.1007/BF02344885.
19. **Jansma JM, Ramsey NF, Coppola R, Kahn RS.** Specific versus nonspecific brain activity in a parametric N-back task. *Neuroimage* 12: 688–697, 2000. doi:10.1006/nimg.2000.0645.
20. **Jasdzewski G, Strangman G, Wagner J, Kwong KK, Poldrack RA, Boas DA.** Differences in the hemodynamic response to event-related motor and visual paradigms as measured by near-infrared spectroscopy. *Neuroimage* 20: 479–488, 2003. doi:10.1016/S1053-8119(03)00311-2.
21. **Kainerstorfer JM, Sassaroli A, Tgavalekos KT, Fantini S.** Cerebral autoregulation in the microvasculature measured with near-infrared spectroscopy. *J Cereb Blood Flow Metab* 35: 959–966, 2015. doi:10.1038/jcbfm.2015.5.
22. **Keshmiri S, Sumioka H, Yamazaki R, Ishiguro H.** A non-parametric approach to the overall estimate of cognitive load using NIRS time series. *Front Hum Neurosci* 11: 15, 2017. doi:10.3389/fnhum.2017.00015.
23. **Kiguchi M, Funane T.** Algorithm for removing scalp signals from functional near-infrared spectroscopy signals in real time using multidistance optodes. *J Biomed Opt* 19: 110505, 2014. doi:10.1117/1.JBO.19.11.110505.
24. **Kirchner WK.** Age differences in short-term retention of rapidly changing information. *J Exp Psychol* 55: 352–358, 1958. doi:10.1037/h0043688.
25. **Krite Svanberg E, Wollmer P, Andersson-Engels S, Åkeson J.** Physiological influence of basic perturbations assessed by non-invasive optical techniques in humans. *Appl Physiol Nutr Metab* 36: 946–957, 2011. doi:10.1139/h11-119.
26. **Mader TH, Gibson CR, Pass AF, Kramer LA, Lee AG, Fogarty J, Tarver WJ, Dervay JP, Hamilton DR, Sargsyan A, Phillips JL, Tran D, Lipsky W, Choi J, Stern C, Kuyumjian R, Polk JD.** Optic disc edema, globe flattening, choroidal folds, and hyperopic shifts observed in astronauts after long-duration space flight. *Ophthalmology* 118: 2058–2069, 2011. doi:10.1016/j.ophtha.2011.06.021.
27. **Michel V, Mazzola L, Lemesle M, Vercueil L.** Long-term EEG in adults: sleep-deprived EEG (SDE), ambulatory EEG (Amb-EEG), and long-term video-EEG recording (LTVER). *Neurophysiol Clin* 45: 47–64, 2015. doi:10.1016/j.neucli.2014.11.004.
28. **Morris D, Schazmann B, Wu Y, Coyle S, Brady S, Fay C, Hayes J, Lau KT, Wallace G, Diamond D.** Wearable technology for bio-chemical analysis of body fluids during exercise. *Conf Proc IEEE Eng Med Biol Soc* 2008: 5741–5744, 2008. doi:10.1109/IEMBS.2008.4650518.
29. **Naschitz JE, Bezobchuk S, Mussafia-Priselac R, Sundick S, Dreyfuss D, Khorshidi I, Karidis A, Manor H, Nagar M, Peck ER, Peck S, Storch S, Rosner I, Gaitini L.** Pulse transit time by R-wave-gated infrared photoplethysmography: review of the literature and personal experience. *J Clin Monit Comput* 18: 333–342, 2004. doi:10.1007/s10877-005-4300-z.
30. **Nybo L, Rasmussen P.** Inadequate cerebral oxygen delivery and central fatigue during strenuous exercise. *Exerc Sport Sci Rev* 35: 110–118, 2007. doi:10.1097/jes.0b013e3180a031ec.
31. **Robertson FC, Douglas TS, Meintjes EM.** Motion artifact removal for functional near-infrared spectroscopy: a comparison of methods. *IEEE Trans Biomed Eng* 57: 1377–1387, 2010. doi:10.1109/TBME.2009.2038667.
32. **Saager R, Berger A.** Measurement of layer-like hemodynamic trends in scalp and cortex: implications for physiological baseline suppression in functional near-infrared spectroscopy. *J Biomed Opt* 13: 034017, 2008. doi:10.1117/1.2940587.
33. **Salmon E, Van der Linden M, Collette F, Delfiore G, Maquet P, Degueldre C, Luxen A, Franck G.** Regional brain activity during working memory tasks. *Brain* 119: 1617–1625, 1996. doi:10.1093/brain/119.5.1617.
34. **Schmitz CH, Locker M, Lasker JM, Hielscher AH, Barbour RL.** Instrumentation for fast functional optical tomography. *Rev Sci Instrum* 73: 429–439, 2002. doi:10.1063/1.1427768.
35. **Scholkmann F, Kleiser S, Metz AJ, Zimmermann R, Mata Pavia J, Wolf U, Wolf M.** A review on continuous wave functional near-infrared spectroscopy and imaging instrumentation and methodology. *Neuroimage* 85: 6–27, 2014. doi:10.1016/j.neuroimage.2013.05.004.
36. **Siebenmann C, Rasmussen P.** Does cerebral hypoxia facilitate central fatigue? *Exp Physiol* 101: 1173–1177, 2016. doi:10.1113/EP085640.
37. **Song J, Xu L, Li J, Xue J, Dong Y, Li X, Zeng H.** Monolayer and few-layer all-inorganic perovskites as a new family of two-dimensional semiconductors for printable optoelectronic devices. *Adv Mater* 28: 4861–4869, 2016. doi:10.1002/adma.201600225.
38. **Steinmetz H, Fürst G, Meyer BU.** Craniocerebral topography within the international 10-20 system. *Electroencephalogr Clin Neurophysiol* 72: 499–506, 1989. doi:10.1016/0013-4694(89)90227-7.

39. **Strangman G, Boas DA, Sutton JP.** Non-invasive neuroimaging using near-infrared light. *Biol Psychiatry* 52: 679–693, 2002. doi:10.1016/S0006-3223(02)01550-0.
40. **Strangman G, Culver JP, Thompson JH, Boas DA.** A quantitative comparison of simultaneous BOLD fMRI and NIRS recordings during functional brain activation. *Neuroimage* 17: 719–731, 2002. doi:10.1006/nimg.2002.1227.
41. **Strangman GE, Li Z, Zhang Q.** Depth sensitivity and source-detector separations for near-infrared spectroscopy based on the Colin27 brain template. *PLoS One* 8: e66319, 2013. doi:10.1371/journal.pone.0066319.
42. **Strangman GE, Zhang Q, Li Z.** Scalp and skull influence on near-infrared photon propagation in the Colin27 brain template. *Neuroimage* 85: 136–149, 2014. doi:10.1016/j.neuroimage.2013.04.090.
43. **Strangman GE, Zhang Q, Marshall-Goebel K, Mulder E, Stevens B, Clark JB, Bershad EM.** Increased cerebral blood volume pulsatility during head-down tilt with elevated carbon dioxide: the SPACECOT Study. *J Appl Physiol (1985)* 123: 62–70, 2017. doi:10.1152/japplphysiol.00947.2016.
44. **Szufladowicz E, Maniewski R, Kozluk E, Zbiec A, Nosek A, Walczak F.** Near-infrared spectroscopy in evaluation of cerebral oxygenation during vasovagal syncope. *Physiol Meas* 25: 823–836, 2004. doi:10.1088/0967-3334/25/4/004.
45. **Villringer A.** Understanding functional neuroimaging methods based on neurovascular coupling. *Adv Exp Med Biol* 413: 177–193, 1997. doi:10.1007/978-1-4899-0056-2_20.
46. **Vogiatzis I, Louvaris Z, Habazettl H, Andrianopoulos V, Wagner H, Roussos C, Wagner PD, Zakynthinos S.** Cerebral cortex oxygen delivery and exercise limitation in patients with COPD. *Eur Respir J* 41: 295–301, 2013. doi:10.1183/09031936.00016312.
47. **Wang Z, Yang Z, Dong T.** A review of wearable technologies for elderly care that can accurately track indoor position, recognize physical activities and monitor vital signs in real time. *Sensors (Basel)* 17: 17, 2017. doi:10.3390/s17020341.
48. **Watenpaugh DE, Hargens AR.** The cardiovascular system in microgravity. In: *Handbook of Physiology*. Bethesda, MD: American Physiological Society, 1996, p. 631–674.
49. **Xu H, Li J, Leung BHK, Poon CCY, Ong BS, Zhang Y, Zhao N.** A high-sensitivity near-infrared phototransistor based on an organic bulk heterojunction. *Nanoscale* 5: 11850–11855, 2013. doi:10.1039/c3nr03989g.
50. **Xu Y, Pei Y, Graber HL, Barbour RL.** Image quality improvement via spatial deconvolution in optical tomography: time-series imaging. *J Biomed Opt* 10: 051701, 2005. doi:10.1117/1.2103747.
51. **Yu L, Xiong D, Guo L, Wang J.** A remote quantitative Fugl-Meyer assessment framework for stroke patients based on wearable sensor networks. *Comput Methods Programs Biomed* 128: 100–110, 2016. doi:10.1016/j.cmpb.2016.02.012.
52. **Zhang LF, Hargens AR.** Intraocular/intracranial pressure mismatch hypothesis for visual impairment syndrome in space. *Aviat Space Environ Med* 85: 78–80, 2014. doi:10.3357/ASEM.3789.2014.
53. **Zhang Q, Brown EN, Strangman GE.** Adaptive filtering for global interference cancellation and real-time recovery of evoked brain activity: a Monte Carlo simulation study. *J Biomed Opt* 12: 044014, 2007. doi:10.1117/1.2754714.
54. **Zhang Q, Brown EN, Strangman GE.** Adaptive filtering to reduce global interference in evoked brain activity detection: a human subject case study. *J Biomed Opt* 12: 064009, 2007. doi:10.1117/1.2804706.
55. **Zhang Q, Ivkovic V, Hu G, Strangman GE.** Twenty-four-hour ambulatory recording of cerebral hemodynamics, systemic hemodynamics, electrocardiography, and actigraphy during people's daily activities. *J Biomed Opt* 19: 47003, 2014. doi:10.1117/1.JBO.19.4.047003.
56. **Zhang Q, Yan X, Strangman GE.** Development of motion resistant instrumentation for ambulatory near-infrared spectroscopy. *J Biomed Opt* 16: 087008, 2011. doi:10.1117/1.3615248.
57. **Zhao G, Mei Z, Liang D, Ivanov K, Guo Y, Wang Y, Wang L.** Exploration and implementation of a pre-impact fall recognition method based on an inertial body sensor network. *Sensors (Basel)* 12: 15,338–15,355, 2012. doi:10.3390/s121115338.